Journal of Ultrafine Grained and Nanostructured Materials
https://jufgnsm.ut.ac.ir
Vol. 58, No.2, June 2025, pp. 242-254
Print ISSN: 2423-6845 Online ISSN: 2423-6837
DOI: 10.22059/jufgnsm.2025.02.09

Effect of Boron Doping on the Structure and Band Gap of ZnO Nanowires Grown by Anodizing: Toward Water Splitting Applications

Samaneh Bordbar[1], Dr. Shahin Khameneh Asl[1], Dr. Shahab Khameneh Asl[1]*, Hakimeh Ghazaie[1], Mobin Dehkharghani[1]

[1] Department of Materials Engineering, Faculty of Mechanical Engineering, University of Tabriz, Tabriz 51666–16471, Iran

Recieved: 1 August 2025; Accepted: 8 October 2025

**Corresponding author, E-mail:* sh.kh.asl@tabrizu.ac.ir

ABSTRACT

Zinc oxide (ZnO) nanowires are promising for solar-driven hydrogen production, but their wide band gap (≈3.3 eV) limits absorption to the ultraviolet (UV) region. This study investigates the effect of boron (B) doping on the structural and optical properties of ZnO nanowires to enhance their photocatalytic potential. ZnO nanowires were synthesized by anodizing high-purity zinc foil in a sodium bicarbonate/ethylene glycol electrolyte at 5 V and 29 °C for 40 min under ambient pressure, followed by annealing at 200 °C. Boron doping was performed by immersion in boric acid (0.025–0.1 M) for 1–10 h, followed by annealing at 250 °C. Characterization using field-emission scanning electron microscopy (FE-SEM), energy-dispersive X-ray spectroscopy (EDX), X-ray diffraction (XRD), Fourier-transform infrared spectroscopy (FTIR), and diffuse reflectance spectroscopy (DRS) revealed that boron content increased from 0 at.% to 23.02 at.% with immersion time and varied from 8.22 at.% to 14.87 at.% with boric acid concentration. Doping increased nanowire diameter from 65.3 nm to 113.8 nm (≈74.4%) and length from 4.63 µm to 4.85 µm (≈4.7%), while reducing the surface-to-volume ratio by ≈36.6%. The optical band gap decreased up to ≈24.2%, enhancing visible-light absorption. These results demonstrate that boron-doped ZnO nanowires exhibit improved light harvesting and structural properties, making them efficient candidates for photocatalytic and photoelectrochemical hydrogen generation under solar illumination.

Keywords: *Zinc oxide; Anodization; Photocatalysis; Hydrogen production; Nanooxide coating, Boron-doped.*

1. Introduction

The global push for sustainable and clean energy sources has intensified interest in hydrogen production through water splitting. As a zero-emission and energy-dense fuel, hydrogen holds significant promise for future energy systems. Semiconductor-based photocatalytic and photoelectrochemical (PEC) water splitting is a widely explored method for converting solar energy into hydrogen using photoactive materials [1]. Several oxide semiconductors such as TiO_2, Fe_2O_3, and WO_3 have been widely explored for water splitting applications due to their abundance, stability, and non-toxicity. However, these materials often exhibit limited photocatalytic efficiency under solar illumination, which has motivated the search for more tunable and structurally adaptable alternatives [2]. Zinc oxide (ZnO) is one such promising candidate. It is a chemically stable and cost-effective n-type semiconductor with high electron mobility and the ability to be synthesized in well-aligned nanowire arrays, which are advantageous for directional charge transport and increased surface area [3]. However, ZnO suffers from a wide direct band gap (~3.3 eV), restricting its activity to the ultraviolet

region of the solar spectrum. This limitation can be addressed through elemental doping, which allows modification of the band structure to extend light absorption into the visible range [4]. Among various dopants, boron has attracted interest due to its small ionic radius, high electronegativity, and ability to incorporate into the ZnO lattice, either substitutionally or interstitially. Boron doping slightly reduces the band gap of ZnO nanowires, extending light absorption modestly into the visible range, while introducing shallow donor states that enhance charge separation and suppress electron–hole recombination, improving photocatalytic efficiency under solar illumination [5]. Compared to other dopants, boron offers a favorable balance of advantages and limitations. Nitrogen doping can more strongly narrow the band gap and enhance visible-light absorption, but often introduces deep trap states that act as recombination centers and may compromise reproducibility [6]. Hydrogen doping enhances carrier density and passivates intrinsic defects, but excessive hydrogen can destabilize the lattice over time [7]. Transition metals such as Cu, Ni, or Co introduce mid-gap states to improve visible-light absorption but frequently induce lattice distortion and defects, which can reduce structural integrity [8]. Rare-earth elements improve visible-light response and charge separation but require more complex synthesis and may increase structural complexity [9]. Overall, boron's combination of moderate band gap reduction, improved charge separation, and maintained structural integrity makes it a highly suitable dopant for ZnO nanowires in solar-driven water splitting applications. The ZnO nanowires in this study were synthesized using the anodizing method, which offers the advantages of simplicity, cost-effectiveness, good vertical alignment, and uniform nanowire arrays. However, anodizing may provide limited control over nanowire diameter and surface defects, and requires careful optimization of voltage and electrolyte composition to achieve reproducible results [10]. Previous experimental works have demonstrated that boron doping of ZnO nanowires can reduce the band gap from ~3.3 eV to as low as 2.5–2.7 eV, enhance visible-light absorption, and improve hydrogen evolution rates under solar irradiation. These studies confirm the practical effectiveness of boron doping but leave open questions about the combined effects of doping duration and concentration on structural and optical properties. The novelty of this work lies in systematically investigating how different boron concentrations and doping durations affect the structure, morphology, and band gap of anodized ZnO nanowires. By correlating boron content with nanowire properties, this study provides insights into optimizing boron-doped ZnO for efficient photocatalytic and PEC water splitting applications. The resulting nanostructures were characterized by FE-SEM, EDX, XRD, FTIR, and DRS to evaluate morphology, crystalline structure, bonding environments, and optical band gap.

2. Experimental

2.1. Preparation of samples

High-purity zinc foil (99.95%, 1 mm thick) was used as the substrate material for ZnO nanowire synthesis. The foils were cut into 1 × 3 cm^2 pieces and polished with abrasive papers of grit sizes ranging from 400 to 2500. Then cleaned sequentially by ultrasonication in acetone, ethanol (each for 15 minutes), and finally electropolished inside ethanol and phosphoric acid electrolyte [11]. After drying under ambient conditions, the foils were prepared for anodizing. The chemical composition of the zinc sheet used as the substrate is listed in Table 1.

2.2. Synthesis of ZnO nanowires via Anodizing

ZnO nanowires were synthesized using an anodizing method in a two-electrode system. The anodizing electrolyte consisted of 50 mM sodium bicarbonate and 10 vol% ethylene glycol. The anodizing process was carried out for 40 minutes at a constant potential of 5 V and a temperature of 29 °C under ambient pressure. The voltage of 5 V was selected to ensure stable and uniform nanowire growth without excessive dissolution or breakdown, while the mild temperature (29 °C) minimized thermal stress and uncontrolled nucleation. The anodizing duration of 40 min was chosen as an optimized condition that allows sufficient vertical growth of ZnO nanowires while preventing overgrowth or structural collapse. Zinc foil with purity of 99.95% was used as the anode, while graphite was used as the cathode due to its high conductivity and chemical inertness in the electrolyte. The graphite cathode was a flat plate with dimensions of approximately 2 × 3 cm^2 and 2 mm thickness, positioned parallel to the zinc anode. The interelectrode gap was maintained at about 2 cm to ensure uniform electric field distribution and reproducible growth conditions. After completion of the synthesis, the samples were rinsed first with distilled water and then with ethanol to remove any residual electrolyte.

Optimization of anodizing parameters: Preliminary trials and literature evidence guided the choice of these conditions. Lower voltages (< 5 V) produced incomplete oxide layers with poor nanowire alignment, whereas higher voltages (> 10 V) caused rapid dissolution and instability of the oxide film. Short anodizing durations (< 20 min) resulted in thin and non-uniform coatings, while excessively long durations (> 60 min) led to overgrowth and partial collapse of the

nanostructures. Likewise, temperatures above 40 °C accelerated dissolution and defect formation, whereas lower temperatures slowed the kinetics and limited vertical growth. Therefore, the selected parameters (5 V, 29 °C, 40 min) provided the optimum balance between nanowire alignment, structural integrity, and reproducibility.

2.3. Heat-treatment of ZnO nanowires

The annealing process was carried out in a tube furnace at 200°C for 2 hours with a heating rate of 2°C/min in air under ambient pressure. After annealing, the samples were allowed to cool naturally inside the furnace to room temperature. The schematic representation of the anodizing setup and nanowire formation process is shown in Fig. 1, while the overall synthesis route of the ZnO nanowires including anodizing and heat treatment steps is summarized in Fig. 2.

2.4. Boron Doping Mechanism

To reduce the band gap energy, the synthesized ZnO nanostructures were subjected to boron doping treatment. For this purpose, the samples were immersed for 1, 2, 5, and 10 hours in aqueous solutions of boric acid (H_3BO_3) with concentrations of 0.025, 0.05, 0.075, and 0.1 M, respectively. These durations were selected to systematically evaluate the effect of diffusion time on boron incorporation into the ZnO lattice, ranging from short-term surface adsorption (1 h) to extended bulk diffusion (10 h). The chosen concentrations were designed to cover a low-to-high precursor range, enabling assessment of both limited incorporation at low levels (0.025 M) and possible saturation or defect formation at higher levels (0.1 M). Such a range allowed us to identify the optimum balance between sufficient boron incorporation and preservation of ZnO crystallinity. After doping, the samples were then thoroughly rinsed with deionized water and dried. Finally, the doped samples were annealed at 250°C for 1 hour with a heating rate of 2°C/min in air under ambient pressure, followed by natural cooling inside the furnace to room temperature.

Table. 1- Chemical composition of the Zn sheet

Element	Percentage(%)
Zn	99.95
Ti	0.002
Ni	0.002
Mg	0.03
Fe	0.031
Cu	0.006

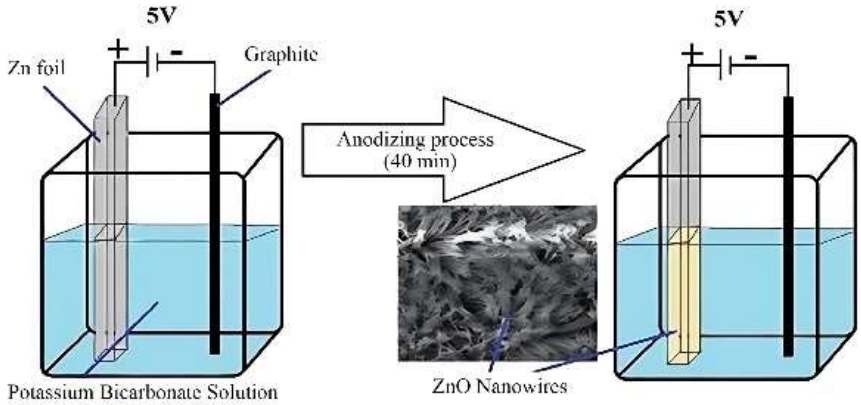

Fig. 1- Schematic illustration of the anodizing process.

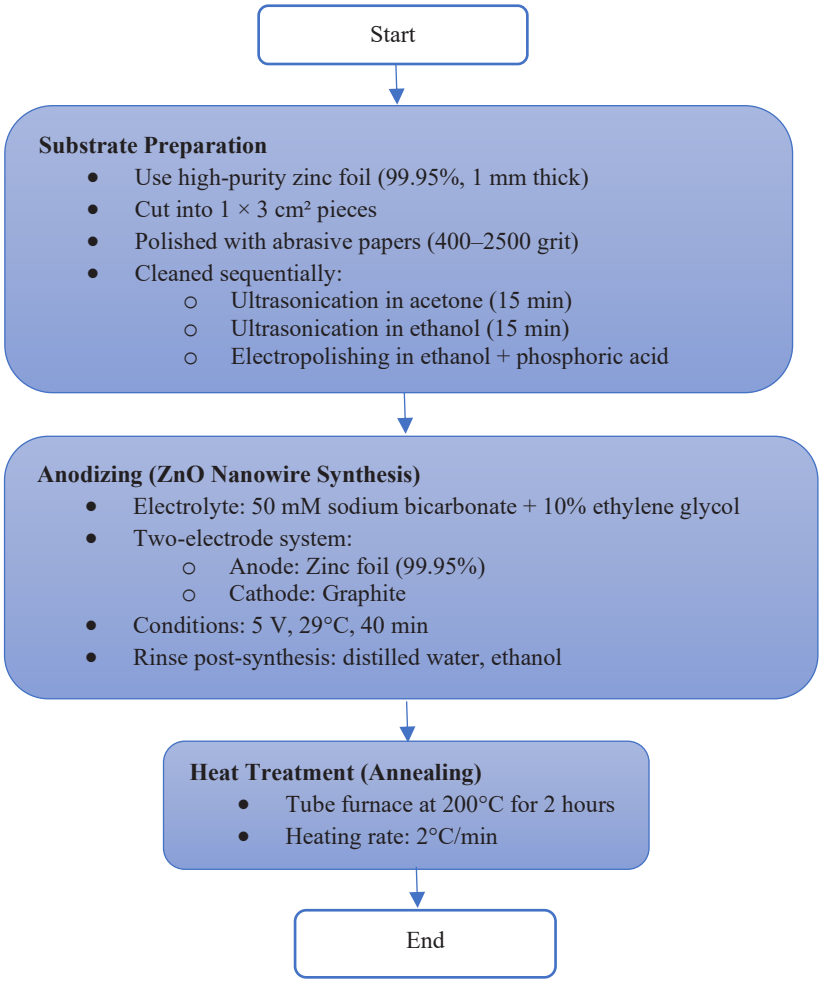

Fig. 2- Flowchart of ZnO nanowire synthesis via.

2.5. Characterization Techniques

The surface morphology and nanowire dimensions were examined using a field emission scanning electron microscope (FE-SEM, TESCAN MIRA III). The elemental composition and boron content were determined by energy dispersive X-ray spectroscopy (EDX) attached to the FE-SEM [12].

X-ray diffraction (XRD) analysis was performed using a Philips PW 730 diffractometer with Cu Kα radiation (λ = 1.5406 Å) in the 2θ range of 20°–80° with a step size of 0.05° and a counting time of 1 s per step to assess the crystallinity and phase composition [13].

Fourier-transform infrared spectroscopy (FTIR, Beam Gostar Taban Company, Tehran, Iran) was used to investigate the chemical bonding and identify functional groups in the synthesized nanowires. Spectra were recorded in the wavenumber range of 400–4000 cm^{-1} [14].

The optical properties and band gap values were measured using diffuse reflectance spectroscopy (DRS) with a UV-Vis spectrophotometer (Shimadzu UV-2600, Japan) equipped with an integrating sphere, located at the Central Laboratory of the University. The optical band gaps were calculated using Tauc plots derived from the Kubelka–Munk function [15]. The sequence of the boron-doping and post-annealing steps is summarized schematically in Fig. 3.

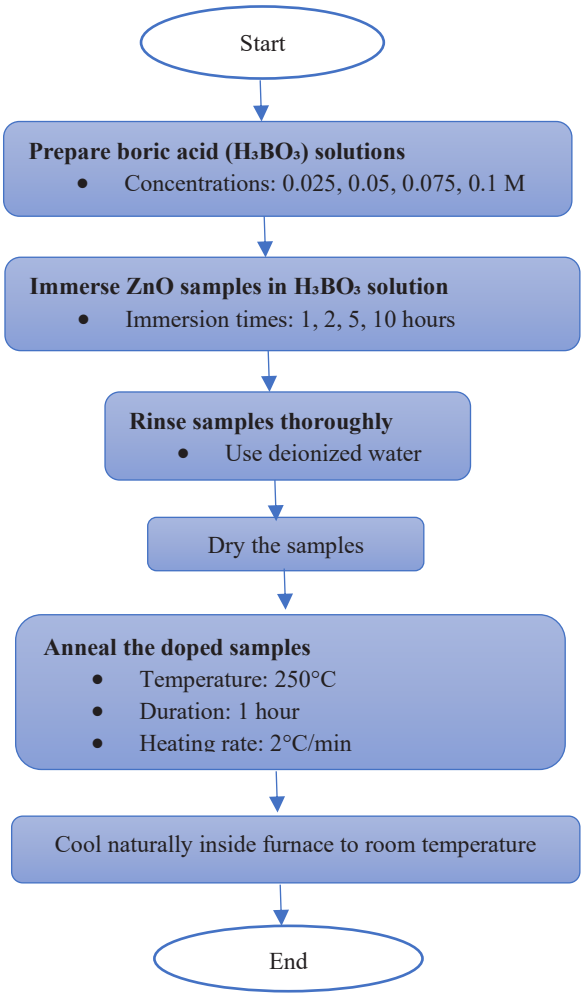

Fig. 3- Flowchart Boron doping mechanism.

3. Results and discussion

3.1. Structural properties

X-ray diffraction (XRD) was performed on both undoped and boron-doped ZnO nanowire samples to analyze their crystal structures. The measurements were conducted using monochromatic Cu Kα radiation (λ = 1.5418 Å) over a 2θ range of 20° to 80°, with a step size of 0.05° and a counting time of 1 s per step. The resulting diffraction patterns, presented in Figures 4 and 5, display characteristic ZnO peaks at 2θ angles of 31.5°, 34°, 35.95°, 42.85°, 54.15°, 56.5°, and 69.8°, corresponding to the (100), (002), (101), (102), (103), (200), and (112) planes, respectively. The observed structural features are also influenced by the anodizing conditions, which affect nanowire alignment and nucleation density [16].

After annealing at 200 °C for 2 hours, the diffraction peaks matched JCPDS card No. 36-1451 [17], confirming a hexagonal wurtzite structure. The wurtzite structure leads to the formation of a white polycrystalline coating. The presence of a strong (112) peak, (highlighted by a red oval in Fig. 5), indicates a preferred orientation along the c-axis, perpendicular to the substrate. No additional peaks related to secondary phases were observed, suggesting high purity of the samples. Although boron doping did not change the overall crystal structure, it affected the relative intensities and sharpness of certain peaks, reflecting subtle changes in crystallinity and lattice strain. At low boron concentrations (0.05 M), the (102) peak, (highlighted by an orange oval in Fig. 4), remained relatively unchanged, indicating limited

lattice distortion. However, with longer doping durations, increased surface oxidation can partially hinder boron incorporation, resulting in a gradual reduction of the (101) peak, (highlighted by a blue oval in Fig. 4), intensity [18]. The observed peak modifications can be explained mechanistically: substitution of Zn atoms with smaller boron atoms introduces compressive strain in the lattice, while high nucleation density at elevated boron concentrations promotes internal stress. Additionally, interstitial incorporation of boron atoms contributes to lattice distortion. These structural strains can influence electron–phonon interactions and defect states, which are important factors affecting the optical and photocatalytic properties of the ZnO nanowires. Although Figures 4 and 5 display the diffractograms only for the shortest and longest immersion durations (1 h and 10 h) and for the lowest and highest precursor concentrations (0.025 M and 0.1 M), the intermediate samples (2 h, 5 h, 0.05 M, and 0.075 M) exhibited the same diffraction peaks with gradual variations in intensity and sharpness. Therefore, the presented patterns can be considered representative of the entire series without unnecessary redundancy.

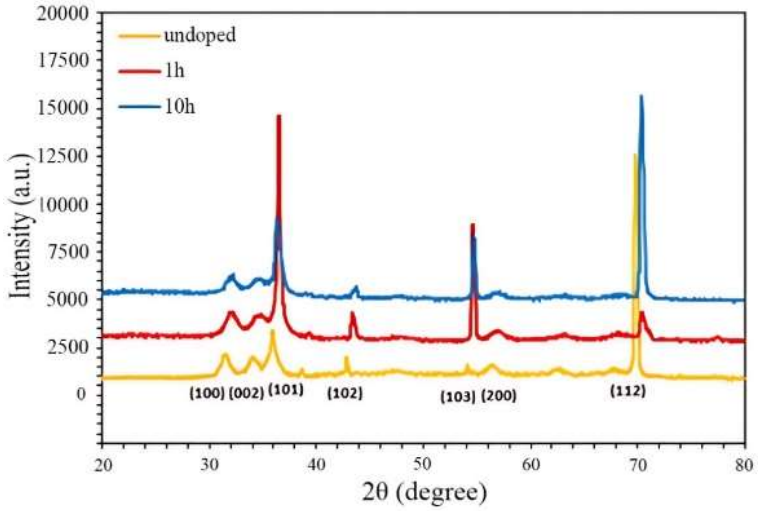

Fig. 4- The diffraction patterns of undoped and doped samples after 1 and 10 hours.

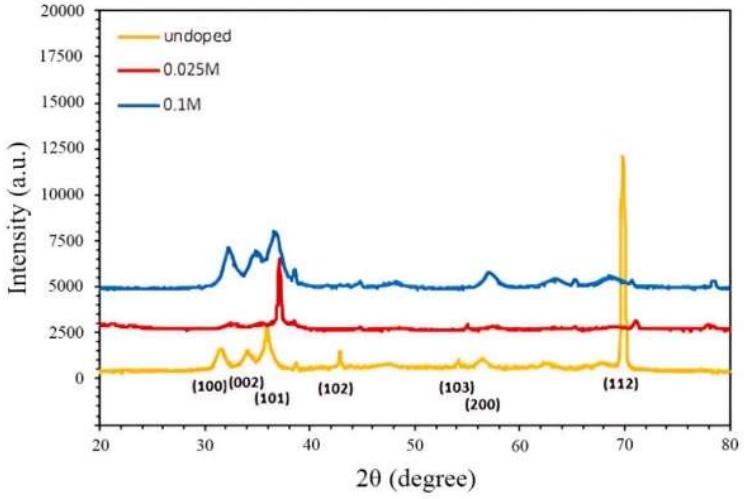

Fig. 5- The diffraction patterns of undoped and doped samples at 0.025 M and 0.1 M concentrations.

3.2. Surface Morphology

FE-SEM images of the top surface and cross-section of the synthesized samples, obtained via the anodizing process and boron doping, are shown in Figures 6 and 7. The nanowire diameter, length, and surface-to-volume ratio were estimated using Clemex software. The measured dimensions of the undoped and boron-doped ZnO nanowires are summarized in Table 2. Both undoped and boron-doped samples were prepared under identical anodizing conditions (5 V, 40 minutes). Specifically, the applied voltage and anodizing duration control the nucleation rate and growth kinetics, promoting vertical alignment, uniform diameter, and defined tip morphology, while the electrolyte composition affects ionic mobility and local supersaturation, influencing nanowire uniformity [19]. As seen in Figure 6-b, the anodized ZnO coatings exhibit a vertically aligned nanowire structure with relatively uniform distribution. The nanowires grow from defined nucleation sites, as indicated by a red arrow. Upon boron doping, the average nanowire diameter increased from 65.30 nm to 113.80 nm, which can be attributed to grain growth and lattice expansion induced by boron incorporation. The nanowire length increased slightly from 4.63 µm (undoped) to 4.85 µm (after 10 hours of doping), indicating that doping duration moderately influences axial growth. This axial growth enhancement likely arises from boron modifying surface energy and facilitating preferential vertical growth at nucleation sites. Nanowire growth initiates when zinc and oxygen concentrations reach a critical level; insufficient local concentrations result in random orientation [20]. The well-aligned structure observed here confirms that anodizing parameters were optimal. Boron-doped nanowires display hemispherical tips, as highlighted in Figure 7-a, suggesting that boron incorporation alters tip morphology, possibly by modifying local diffusion kinetics or surface tension at the nanowire apex. These morphological changes are expected to influence surface area, light absorption, and charge separation, which are critical for photocatalytic performance [21].

Although Figures 6 and 7 present the FE-SEM images for undoped ZnO and the longest doping duration (10 h), as well as for the lowest and highest precursor concentrations, the intermediate samples (2 h, 5 h, 0.05 M, and 0.075 M) exhibited similar morphological features with gradual increases in diameter and slight variations in tip shape. Therefore, the representative images shown here capture the overall trend of boron-induced grain growth and morphology evolution without redundancy.

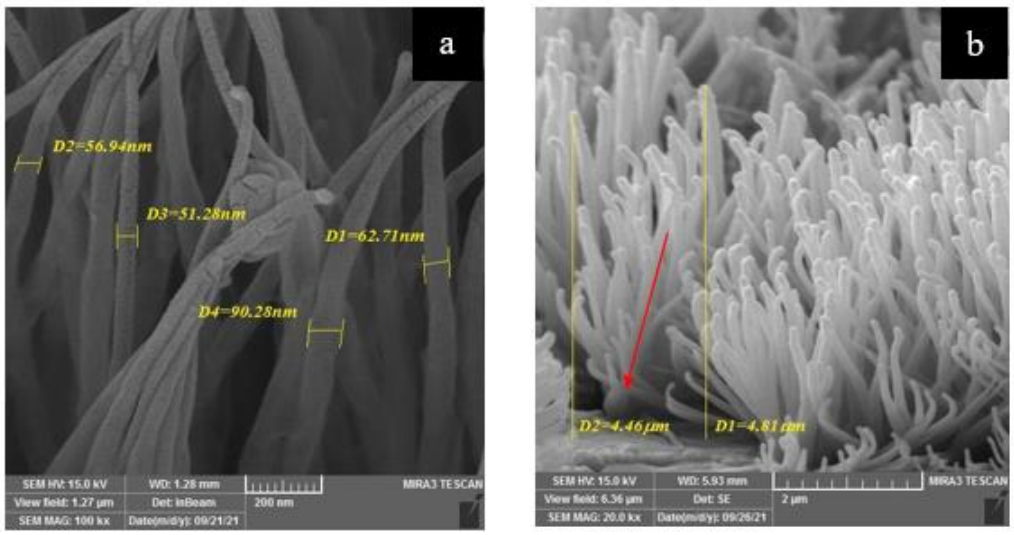

Fig. 6- (a) FE-SEM images of the anodized coating in top view under conditions of 5 volts and 40 minutes at high magnification; (b) cross-section of the coating.

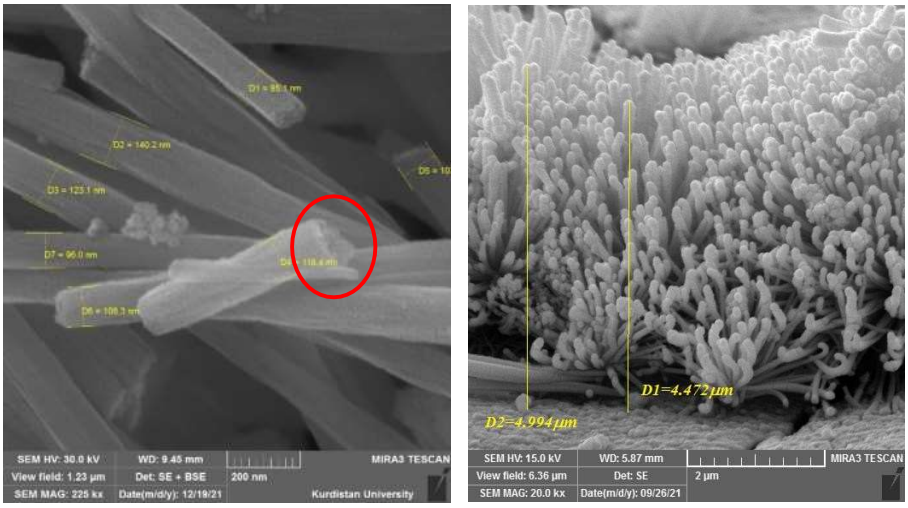

Fig. 7- (a) FE-SEM images of the doped coating in top view under conditions of 5 volts and 40 minutes at high magnification; (b) cross-section.

Table. 2- Dimensions of the undoped and doped nanowires

Sample	Diameter (nm)	Length (µm)	Surface-to-volume ratio (1/m)
Undoped	**65.30**	**4.63**	**35.03**
Doped	**113.80**	**4.85**	**22.23**

3.3. Elemental Composition

The elemental composition of the ZnO nanowires was investigated using Energy-Dispersive X-ray Spectroscopy (EDX). The spectra confirmed the presence of zinc and oxygen, indicating successful formation of ZnO nanowires during the anodizing process. Boron was detected in all doped samples except the one with a 1-hour doping duration, where its absence is likely due to insufficient diffusion time or a concentration below the detection threshold. As the doping duration increased, the boron content also increased. The corresponding atomic percentages of Zn, O, and B obtained from EDX analysis are summarized in Table 3 .For instance, after 10 hours of doping, boron was clearly detected, indicating a time-dependent diffusion process into the ZnO lattice, as shown in Figure 8-a. Similarly, increasing the boron precursor concentration initially led to higher boron incorporation. However, at 0.1 M, the boron signal decreased significantly (Figure 8-b), suggesting a saturation limit or reduced incorporation efficiency at higher concentrations. This effect may arise from solubility limits, surface desorption, or competitive adsorption sites on the nanowire surface [22]. These compositional results are consistent with the XRD and FE-SEM analyses: progressive boron incorporation led to subtle peak broadening and intensity variations in XRD, reflecting lattice strain, and also correlated with the observed increase in nanowire diameter in FE-SEM. Moreover, the incorporation trend explains the band gap narrowing revealed by DRS, while the reduced efficiency at 0.1 M is consistent with defect formation. These observations suggest that boron incorporation is controlled by both diffusion kinetics and precursor availability, which in turn affects lattice strain, defect formation, and ultimately the optical and photocatalytic properties of the nanowires. Understanding these mechanisms is essential for optimizing doping parameters to achieve desired structural and functional outcomes.

Table. 3- Atomic percent of Zn, O, and B elements

Sample	Undoped	1 hour doped	2 hours doped	5 hours doped	10 hours doped	0.025M doped	0.075M doped	0.1M doped
Zn (at.%)	80.00	87.4	60.85	56.03	60.00	60.29	58.88	65.30
O (at.%)	20.00	12.6	27.24	30.43	16.98	29.82	26.26	26.48
B (at.%)	-	0.0	11.91	13.53	23.02	9.89	14.87	8.22

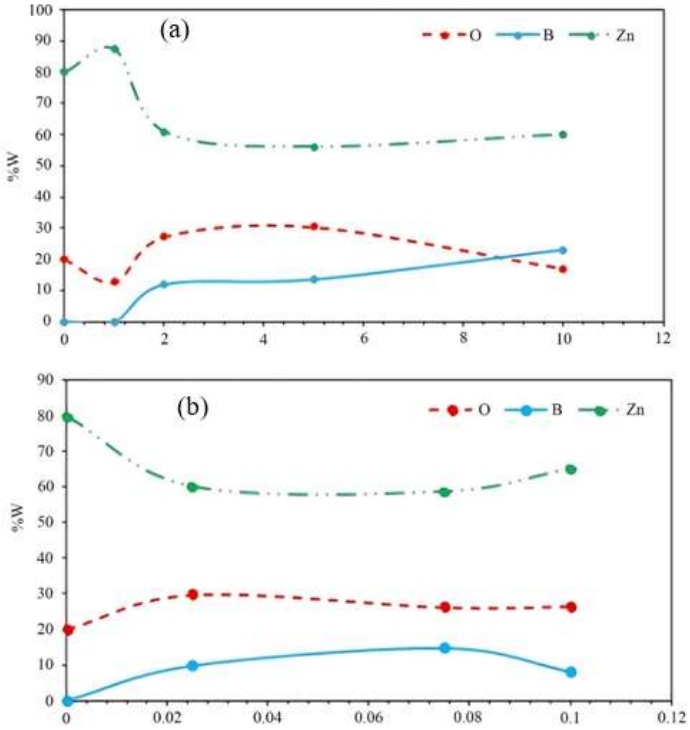

Fig. 8- (a). Comparison of zinc, oxygen, and boron elements at 1, 2, 5, and 10 hours. (b). Comparison of zinc, oxygen, and boron elements at concentrations of 0.025, 0.05, 0.075, and 0.1 molar.

3.4. Optical Properties

The optical properties of undoped and boron-doped ZnO nanowires were investigated using diffuse reflectance spectroscopy (DRS) to determine their optical band gap and light absorption behavior. DRS is a key technique for evaluating electron excitation across the band gap in semiconductors. The absorption spectra as a function of wavelength for undoped and boron-doped ZnO nanowires under UV–visible irradiation at room temperature are presented in Figures 9-a and 9-b. The corresponding Tauc plots of $(\alpha h\nu)^2$ versus photon energy (E_g) are shown in Figures 10-a and 10-b. According to the Beer–Lambert law, the absorption coefficient is related to the transmitted (I) and incident (I_0) light intensities by:

$$\mathbf{I = I_0\, e^{-\alpha L}} \quad (1)$$

where L is the optical path length. Taking the natural logarithm of both sides gives:

$$\boldsymbol{\alpha}= \left(\frac{I_0}{I}\right) Ln\ \frac{1}{L} \quad (2)$$

when absorbance $A= \log_{10}(I_0/I)$ is used instead of the natural logarithm, this relation becomes:

$$\boldsymbol{\alpha}= \frac{2.303A}{L} \quad (3)$$

The photon energy (E) corresponding to a specific wavelength (λ) is obtained using Planck's relation:

$$\mathbf{E = h\nu = \frac{h\nu}{\lambda} = \frac{1240}{\lambda}} \quad (4)$$

where h is Planck's constant (4.1357×10^{-15}eV/cdotps), c is the speed of light (2.998×10^{8}m/s), and λ is the wavelength in nanometers.

The optical band gap (E_g)was determined using the Tauc relation:

$$\mathbf{(\alpha h\nu)^n = A\,(h\nu - }E_g\mathbf{)} \quad (5)$$

where A is a proportionality constant and n=2 for a direct-allowed electronic transition, typical of ZnO. For diffuse reflectance data, α can be replaced by the Kubelka–Munk function F(R), defined as:

$$\mathbf{F(R) = \frac{(1-R)^2}{2R}} \quad (6)$$

Thus, $(F(R)(h\nu)^2$ is plotted versus hν, and the intercept of the linear portion of the curve with the energy axis gives the optical band gap E_g.

Figures 9–10 were processed using Origin 2019. The absorption wavelengths obtained from the diffuse reflectance spectroscopy measurements were first converted to photon energy (hν) using Equation (2). The corresponding absorption coefficient (α) was then calculated using Equation (1) and substituted into $(\alpha h\nu)^2$. With both E_g and $(\alpha h\nu)^2$ available, Tauc plots of $(\alpha h\nu)^2$ versus E_g were constructed. The optical band gap was determined from the intercept of the linear portion of the plot with the energy axis, and the resulting values are summarized in Table 4.

Figure 9-a shows that ZnO nanowires doped for 1 hour exhibit higher optical absorption compared to those doped for 2, 5, and 10 hours. This increased absorption is due to incomplete boron incorporation at 1 hour, where boron atoms deposit on the nanowire surface as isolated atoms or clusters, enhancing light absorption. In Figure 9-b, nanowires doped with 0.1 M boron concentration show greater UV-visible absorption than those doped at 0.025, 0.05, and 0.075 M. The lowest absorption occurs at 0.025 M, likely because of insufficient boron content. Absorption depends on the total surface area, number, and length of the nanowires. Figures 10-a and 10-b present the bandgap values. Boron-doped nanowires exhibit a reduced bandgap of about 2.70 eV, compared to 3.03 eV for undoped nanowires a decrease of 0.32 eV. This reduction is attributed to boron doping, which increases defect density, reduces atomic spacing, and

induces structural disorder, thereby narrowing the optical bandgap [23]. These optical observations are consistent with the EDX and XRD results, where boron incorporation was shown to induce lattice strain and defect formation. Such structural modifications directly explain the observed band gap narrowing and extended light absorption into the visible region. Concurrently, boron incorporation introduces shallow donor states and defect sites, which can temporarily trap photogenerated electrons [24]. These shallow traps reduce electron–hole recombination by spatially separating carriers, allowing holes to participate in oxidation reactions at the nanowire surface while electrons are available for reduction processes. The presence of these defects also increases the density of active sites, enhancing surface-mediated charge transfer to water molecules [25]. Overall, the interplay between band gap narrowing, extended visible-light absorption, and defect-mediated charge separation synergistically improves the efficiency of solar-driven water splitting, highlighting the critical role of controlled boron doping in tuning the photocatalytic performance of ZnO nanowires.

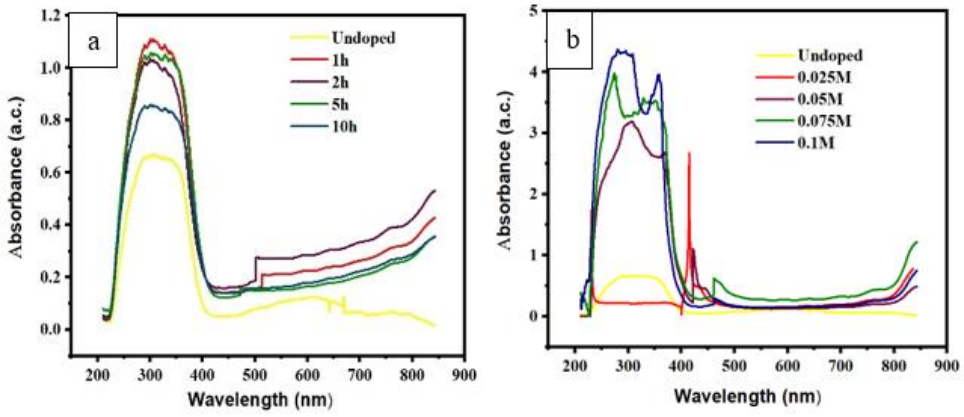

Fig. 9- UV-vis spectra of the doped samples. (a). At different times. (b). At different concentrations.

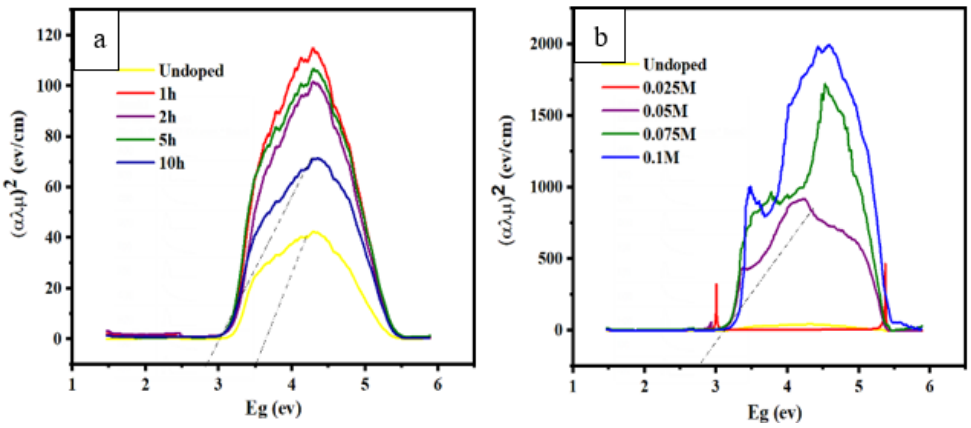

Fig. 10- The $(\alpha hv)^2$ versus Eg curves. (a). At different times. (b). At different concentrations.

Table. 4- The band gap energy values of the undoped and doped sample

Sample	Undoped	1 hour doped	2 hours doped	5 hours doped	10 hours doped	0.025M doped	0.05M doped	0.075M doped	0.1M doped
E_g(eV)	≈3.03	≈2.85	≈2.67	≈2.60	≈2.58	≈2.74	≈2.66	≈2.57	≈2.50

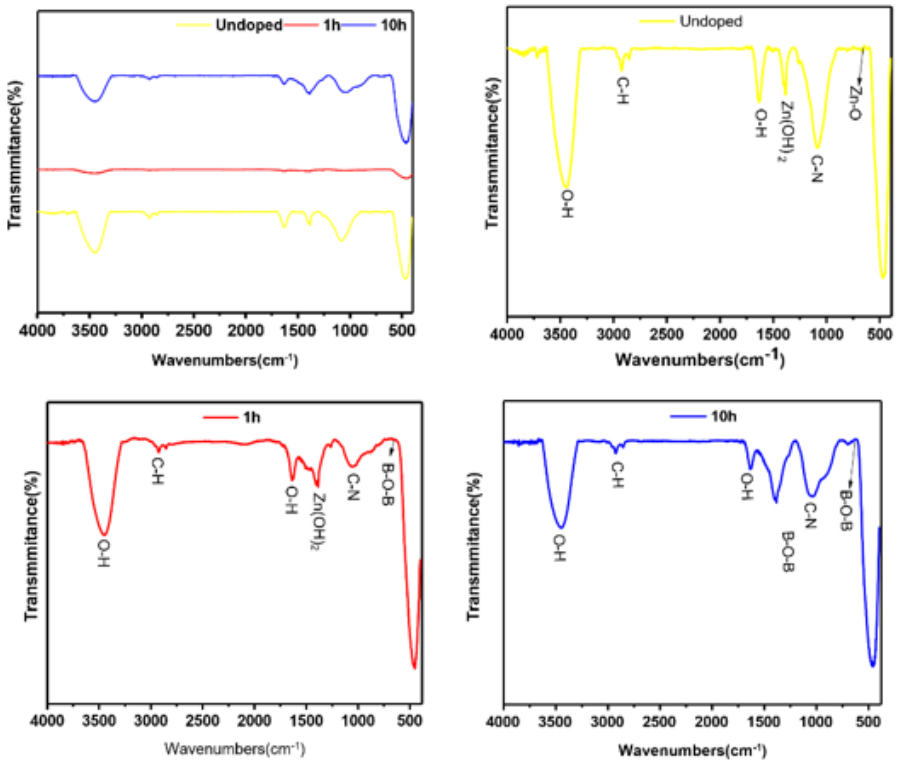

Fig. 11- FTIR spectra of the undoped and doped samples at 1 and 10 hours.

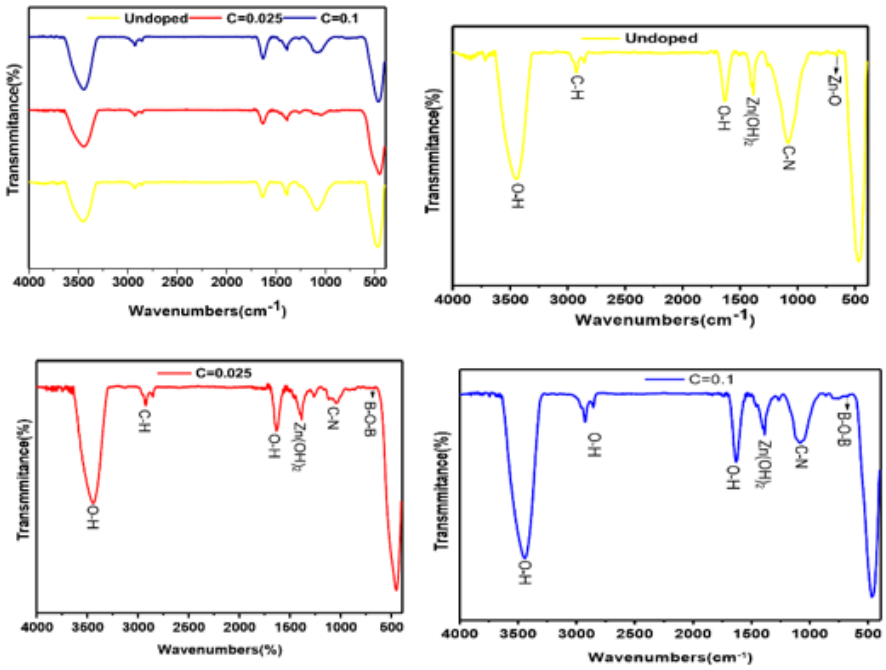

Fig. 12- FTIR spectra of the undoped and doped samples at concentrations of 0.025 and 0.1 molar.

3.5. Functional Group Identification

FTIR spectra of undoped and boron-doped ZnO nanowires are shown in Figures 11 and 12, providing insights into surface functional groups and bonding interactions between boron and ZnO. Measurements were performed at room temperature over the range of 450–4000 cm^{-1}. The absorption peak at 651 cm^{-1} corresponds to Zn–O stretching vibrations, confirming the preservation of the wurtzite crystal structure in both undoped and doped samples. Peaks near 1623 cm^{-1} and 3425 cm^{-1} are attributed to O–H bending and stretching modes, indicating the presence of hydroxyl groups on the nanowire surface, which can act as active sites for adsorption in photocatalytic reactions. The band at 1307 cm^{-1} is associated with C–H vibrations, while the absorption at 513 cm^{-1} corresponds to $Zn(OH)_2$ species, suggesting minor surface hydroxide formation.

Additionally, a peak at 348 cm^{-1} indicates the presence of C–N functional groups, likely from residual synthesis reagents. Importantly, a characteristic peak near 630 cm^{-1} appears only in boron-doped samples, which can be assigned to B–O–B bonding. This confirms the successful interstitial incorporation of boron atoms into the ZnO lattice [26]. Mechanistically, the B–O–B bonds introduce lattice distortions and defect states, which can act as shallow donor levels. These defect states enhance charge separation by trapping efficiency of the doped ZnO nanowires. These results confirm that boron incorporation occurs gradually photogenerated electrons or holes, thereby reducing recombination rates and improving the photocatalytic controlled boron doping in tuning the photocatalytic performance of ZnO nanowires. with both time and concentration, and the resulting B–O–B linkages correlate with the XRD peak broadening and the band gap narrowing observed in DRS. This cross-evidence supports the role of boron doping in tailoring the optical and photocatalytic properties of ZnO nanowires.

4. Conclusions

In this work, undoped and boron-doped ZnO nanowires were successfully synthesized and systematically characterized to evaluate their potential in solar-driven hydrogen production. The main achievements of this study can be summarized as follows:

- Synthesis and Doping Strategy: Vertically aligned ZnO nanowires were successfully synthesized and doped with boron under varying concentrations and durations, confirming a controllable and reproducible fabrication approach.

- Structural stability – XRD analysis confirmed that all samples maintained the hexagonal wurtzite crystal structure after boron incorporation, with the dominant (112) diffraction peak preserved. This demonstrates that boron doping does not disrupt the lattice phase while allowing controlled structural modification .
- Morphological control – FE-SEM observations showed that the nanowires retained their vertical alignment and nanoscale geometry post-doping, with only minor increases in diameter and length attributed to boron-induced grain growth.
- Successful boron incorporation – EDX measurements verified boron presence at higher concentrations and longer doping durations, while FTIR spectra revealed characteristic B–O–B vibrational bands near 630 cm^{-1} alongside Zn–O modes, confirming boron integration at the lattice level.
- Enhanced optical response – DRS and Tauc plot analysis showed a band gap narrowing from 3.03 eV (undoped) to 2.70 eV (boron-doped). This shift modestly extends absorption into the visible range and is attributed to boron-induced defect states and lattice distortions, which facilitate more efficient light harvesting.
- Improved photocatalytic potential – The combined effects of preserved crystallinity, maintained nanowire alignment, and enhanced visible-light absorption suggest improved separation and utilization of photogenerated carriers. These properties are directly beneficial for photocatalytic and photoelectrochemical water splitting, establishing boron-doped ZnO nanowires as promising candidates for solar hydrogen production.

Beyond these findings, this study contributes to the field of photocatalytic hydrogen generation by demonstrating that boron doping provides a practical and structurally stable route for tailoring ZnO nanowires, balancing band gap narrowing with minimal structural disruption. Future research should focus on device-level implementation, stability testing under operating conditions, and co-doping or heterojunction strategies to further enhance performance and accelerate the integration of boron-doped ZnO nanowires into next-generation solar fuel technologies.

References

1. Hisatomi, T.; Domen, K. Photocatalytic Water Splitting for Large-Scale Solar-to-Chemical Energy Conversion and Storage. Frontiers in Science 2024, Article 1411644.
2. Sivula, K.; van de Krol, R. Semiconducting materials for photoelectrochemical energy conversion. Nature Reviews Materials, 2016, 1(2):15010.
3. Ma, M. et al. "Engineering the photoelectrochemical behaviors of ZnO for efficient solar water splitting." Journal of Semiconductors 41 (9), 091702 (2020).
4. Al-Qadasy S, Ahmed A, Khan S, Lee J, Park Y. Effect of boron doping and annealing on the structure, morphological, and optical properties of ZnO films. Physica Scripta. 2024;99(6):0659a3.
5. Wang W, Ai T, Yu Q. Boron-doped nanomaterials for photocatalysis. Applied Catalysis B: Environmental. 2023;300:120708.
6. Ali MARS, Khan M, Singh R, Patel V. Nitrogen-doped ZnO nanowire arrays for photoelectrochemical water splitting. Scientific Reports. 2020;10:12925.
7. Van de Walle, C. G. Hydrogen as a cause of doping in zinc oxide. Physical Review Letters, 2000, 85(5): 1012–1015.
8. Abebe, B.; Gupta, N. K.; Tsegaye, D. A critical mini-review on doping and heterojunction formation in ZnO-based catalysts. RSC Advances (2024) 14, 17338–17349.
9. Kumar, S. G. Lanthanide ions–doped ZnO based photocatalysts: a concise overview of structure–optical effects and activity. Chemical Engineering Journal, 2021.
10. Zaraska, L.; Mika, K.; Syrek, K.; Sulka, G. D. Formation of ZnO Nanowires during Anodic Oxidation of Zinc in Bicarbonate Electrolytes. Journal of Electroanalytical Chemistry 2017, 801, 511–520.
11. Landolt, D. Electrochemical and Materials Aspects of Electropolishing. Electrochimica Acta, 1987, 32 (1): 1–11.
12. Goldstein M, Newbury DE, Joy DC, Lyman CE, Echlin P. Scanning electron microscopy and X-ray microanalysis. 4th ed. Springer; 2017. p. 51–75.
13. Cullity BD, Stock SR. Elements of X-ray diffraction. 3rd ed. Prentice Hall; 2001. p. 110–135.
14. Griffiths PR, de Haseth JA. Fourier transform infrared spectrometry. 2nd ed. Wiley-Interscience; 2007. p. 23–47.
15. Sze SM, Ng KK. Physics of semiconductor devices. 3rd ed. Wiley; 2007. p. 210–215.
16. Masuda R, Kowalski D, Kitano S, Aoki Y, Nozawa T, Habazaki H. Characterization of dark-colored nanoporous anodic films on zinc. Coatings. 2020;10(11):1014.
17. El-Khallawi, M. M. & Hassanien, A. M. (2018). Structural Characterization and Magnetic Properties of Undoped ZnO Nanorods. Journal of Nanomaterials, 2018, Article ID 9072325.
18. Yazıcı Çağlar Y., Ilican S., Çağlar M. FESEM, XRD and DRS studies of electrochemically deposited boron-doped ZnO films. Materials Science in Semiconductor Processing. 2018; 35: 824–832.
19. Ozdemir ET, Kartal U, Dikici T, Erol M, Yurddaskal M. A comparative study on structural, morphological and photocatalytic properties of anodically grown ZnO nanowires under varying parameters. Journal of Materials Science: Materials in Electronics. 2021;32(23):27398–27408.
20. Wang ZL. Zinc oxide nanostructures: Growth, properties and applications. Journal of Physics: Condensed Matter. 2004;16(25):R829–R858.
21. Bagga S, Akhtar J, Mishra S. Synthesis and applications of ZnO nanowire: A review. Journal of Molecular Structure. 2018;20:1–15.
22. Zhao, D., Sathasivam, S., Li, J., & Carmalt, C. J. Transparent and conducting boron-doped ZnO thin films grown by aerosol-assisted CVD. RSC Advances, 12 (2022) 33049–33055.
23. Alsaad A.M., Ahmad A.A., Qattan I.A., Al-Bataineh Q.M., Albataineh Z. Optical properties of undoped ZnO and boron-doped ZnO thin films prepared by sol-gel dip coating. Optik (2020) 211, 164641.
24. Ayoub I., Al-Hada N.M., Abaker M., et al. Advances in ZnO: Manipulation of defects for enhancing properties and applications. Nanotechnology Reviews (De Gruyter), 2022;11(1):1591–1625.
25. Abdul Hamid, S. B.; Teh, S. J.; Pan, G.-T. Photocatalytic Water Oxidation on ZnO: A Review. Catalysts 2017, 7 (3), 93.
26. Boroica, L.; Radu, D.; Medianu, R. FTIR spectra of glasses from $BaO–B_2O_3–TiO_2$ system. Journal of Optoelectronics and Advanced Materials 2008, 10(12), 3218–3221.